

Origin of the enhancement of tunneling probability in the nearly integrable system

Yasutaka Hanada,¹ Akira Shudo,¹ and Kensuke S. Ikeda²

¹*Department of Physics, Tokyo Metropolitan University, Tokyo 192-0397, Japan*

²*Department of Physics, Ritsumeikan University, Kusatsu, Shiga, 525-0577, Japan*

(Dated: June 23, 2018)

The enhancement of tunneling probability in the nearly integrable system is closely examined, focusing on tunneling splittings plotted as a function of the inverse of the Planck's constant. On the basis of the analysis using the absorber which efficiently suppresses the coupling creating spikes in the plot, we found that the splitting curve should be viewed as the staircase-shaped skeleton accompanied by spikes. We further introduce renormalized integrable Hamiltonians, and explore the origin of such a staircase structure by investigating the nature of eigenfunctions closely. It is found that the origin of the staircase structure could trace back to the anomalous structure in tunneling tail which manifests itself in the representation using renormalized action bases. This also explains the reason why the staircase does not appear in the completely integrable system.

PACS numbers: 05.45.Mt, 05.45.-a, 03.65.Xp, 03.65.Sq

I. INTRODUCTION

The tunneling effect is peculiar to quantum mechanics and no counterparts exist in classical mechanics. Quantum tunneling plays a role and actually manifests in various situations ranging from atomic and molecular physics to various phenomena in condensed phases.

In most cases, incorporating the tunneling effect into each case is made by using the system with a single degree of freedom. This is justified and certainly provides a good description if the tunneling penetration proceeds in only one direction, but this is not the case when the system has multi degrees of freedom.

The most important qualitative difference between one- and multi-dimensional systems would be that classical particles are confined not only by the energy barrier, but also by the *dynamical barrier*. The latter is formed when additional constants of motion, either globally or locally, exist besides the energy. What is more crucial is the fact that generic multi-dimensional systems are no more completely integrable and chaos appears in the underlying classical dynamics, so one must take into account new aspects of quantum tunneling absent in completely integrable systems [1, 2].

The role of classical chaos in quantum tunneling has first been discussed in the observation of the wave packet dynamics [3], and then clearly recognized in the behavior of the tunneling splitting of eigenenergies [4–6]. To understand why chaos could play a role in the tunneling process, it suffices to suppose the states forming a doublet, which is a complete analog of the doublet appearing in the system with one-dimensional symmetric double well potential. It is important to note, however, that the doublet in multi-dimensional systems are supported by symmetric regular tori in phase space and chaos exists in between. As one varies an external parameter of the system, it can happen that states forming the doublet and a state supported by the chaotic region come close to each other in the energy space and form avoided crossing. Within the interaction regime, the energy splitting between the

doublet becomes large through couplings with the chaotic state, meaning that the tunneling amplitude between one torus to the other is enhanced. *Chaos-assisted tunneling* (CAT) occurs in this way [4, 5]. A similar enhancement is known to take place if the doublet is bridged by nonlinear resonances. Nonlinear resonances are also important ingredients in multi-dimensional systems, and the latter mechanism is called *resonance-assisted tunneling* (RAT) [7–12].

In order to go beyond qualitative explanations and to obtain more direct evidence for the connection between chaos (and/or nonlinear resonances) semiclassical (WKB) analyses are desired, especially based on the complex classical dynamics since quantum tunneling is a classically forbidden process.

For the system with one degree of freedom, there indeed exists a standard approach that has been established already [13]. The *instanton* is the name of a complex orbit which conveys the tunneling amplitude running along the imaginary time axis, and the formula representing the tunneling splitting in the symmetric double well mode is expressed as

$$\Delta E \sim \alpha \hbar e^{-S/\hbar}, \quad (1)$$

where and classical ingredients α and S can be deduced in the instanton calculation [13].

On the other hand, in multi-dimensional cases, full semiclassical analyses using the complex classical dynamics could so far be applied only to the time domain [14, 15] and have not been even formulated except for completely integrable situations in the energy domain [16–19]. The enhancement of tunneling could therefore be well accounted for in terms of the complex dynamics [20], but fully convincing semiclassical understanding for the energy domain is still lacking.

The aim of this article is to explore the origin of the enhancement of tunneling probability observed in the energy domain. The tunneling probability in the energy domain is often measured by tracking the energy splitting or the properly defined tunneling rate as a function of

$1/h$. The enhancement is typically observed as plateaus accompanied by spikes due to energy resonance [6, 8]. Characteristics observed there are understood within a framework of RAT, and in particular, plateaus could be interpreted as a kind of phenomena that might be called quantum overlapping resonances; a bunching of spikes, each of which is associated with an individual quantum resonance, turns out to create plateaus, or a persistent long-range interaction of each resonance with other states [11, 12].

However, one should recall that the enhancement occurs even when the Planck's constant is not small enough to resolve the chaotic components or nonlinear resonance islands. This rather paradoxical behavior has been already observed in several models [20, 21], but its origin in such a slightly perturbed regime has never been seriously investigated to the authors' knowledge.

We here take a close look at the nature of the enhancement of the tunneling probability in such nearly integrable regimes by introducing techniques such as absorbing the individual states involved in avoided crossings and decomposing the eigenstates into proper integrable bases, as explained in detail below. We especially focus not only on the behavior of the energy levels but also on the nature of eigenfunctions to elucidate which components are mostly responsible for the plateau structure formed in the energy splitting vs $1/h$ plot.

In conjunction with this, we shall stress the importance of observing wavefunctions in the whole range because there are various ways to define the "tunneling probability", and the nature of tunneling may look different depending on how it is defined. Here, for the closed system (standard map) the splitting of energy levels will be adopted to measure the tunneling probability, whereas for the open system, like the Hénon map, the probability in the asymptotic region is naturally introduced, and the decay rate for the absorbed system is sometimes used. There would be no legitimate way or one should even say that providing a proper definition of the tunneling probability itself is an issue to be explored in nonintegrable systems. Therefore, one should examine more carefully the tail of wavefunctions in the whole range before focusing on the amplitude at a certain specific position.

The present analysis is motivated by a recent work in which the mechanism of the *instanton-noninstanton* (I-NI) *transition* has closely been studied in terms of quantum perturbation theory [21], and so spirits and tools for analyses are overall common. The term instanton-noninstanton (I-NI) is named after the first transition at which the deviation from the instanton prediction starts [21].

The organization of the paper is as follows: In section II, we introduce the system studied in this paper, and present aspects of the enhancement of the tunneling probability by observing the quantum number and $1/h$ dependence of the tunneling probability in our model. In section III, introducing an absorbing operator, which projects out a given set of integrable states, we examine

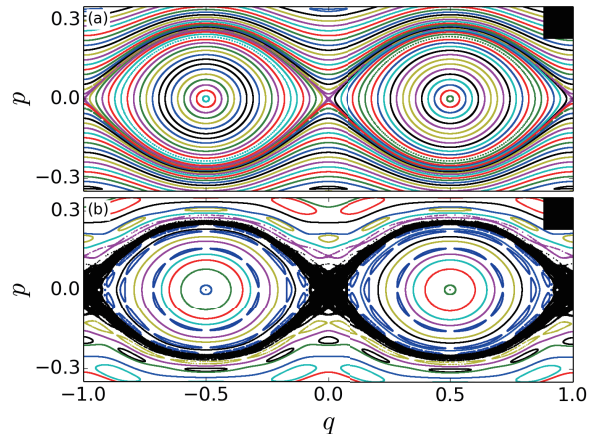


FIG. 1: (Color online) Classical phase space for the symmetrized standard map f with (a) $\tau = 2/3$ and (b) $\tau = 1$. There are no visible resonance chains for $\tau = 2/3$ in the inner tours region while chaotic regions around the unstable fixed point at $(q, p) = (0, 0)$ and some resonance chains (1: 8, 1: 10, 1: 12, ...) become visible for $\tau = 1$. They are shown in dark blue. The black box put in the upper right corner indicates the size of the effective Planck's constant for $h = 1/70$.

which states are responsible for creating spikes typically observed in the splitting curve and whether or not the staircase structure of the splitting curve appears as a result of local quantum resonances in the energy space. In section IV, we investigate the nature of eigenstates to clarify the mechanism of the enhancement by focusing on the local probability amplitude of eigenfunctions and the contribution spectrum introduced in [21]. In section V, on the basis of analyses made in section IV we claim that an essential difference of the splitting curve exists between integrable and nonintegrable systems. In the final section, we summarize and provide outlook especially toward our forthcoming papers.

II. ENHANCEMENT OF TUNNELING PROBABILITY

We consider a quantum system described by the evolution operator in a symmetrized form:

$$\hat{U} = e^{-\frac{i}{\hbar}V(\hat{q})\tau/2} e^{-\frac{i}{\hbar}T(\hat{p})\tau} e^{-\frac{i}{\hbar}V(\hat{q})\tau/2}. \quad (2)$$

The corresponding classical dynamics is given as the symplectic map $f := f_V(\frac{\tau}{2}) \circ f_T(\tau) \circ f_V(\frac{\tau}{2})$ where $f_V(\tau) : (q, p) \mapsto (q, p + \tau V'(q))$ and $f_T(\tau) : (q, p) \mapsto (q + \tau T'(p), p)$ are trivial symplectic maps. Here the prime stands for the derivative of the function. The classical map f corresponds to discretization of the continuous Hamiltonian flow for $H(q, p) = T(p) + V(q)$ up to the second order of the discrete time step τ . Thus, the map f has the integrable (continuous) limit $\tau \rightarrow 0$, and much the same is true on the quantum map (2). Hereafter we take the potential function as $T(p) = p^2/2$ and

$V(q) = (k/4\pi^2) \cos(2\pi q)$ where k is the strength of the perturbation. After rescaling as $p \mapsto p/\tau$ and $k\tau^2 = \varepsilon$, the classical map f turns out to be the symmetrized standard map [22], and the time evolution by the unitary operator \hat{U} can be interpreted as a single period evolution of a δ -functional periodically forcing Hamiltonian with a period τ .

In the continuous limit $\tau \rightarrow 0$, the closed area surrounded by the separatrix is given by $S = \sqrt{k}(2/\pi)^2$. In the following argument, we focus especially on the nearly integrable regime and a proper integrable limit will play an important role as a reference. In most of situations, nonlinearity is controlled by changing the parameter τ , keeping the parameter fixed as $k = k_0 \equiv 0.7458$.

Figure 1 displays classical phase space for typical nearly integrable parameter regions. In the case of $\tau = 2/3$, classical phase space is predominantly covered by regular regions and nonlinear resonance chains are not visible in this scale. For $\tau = 1$, small chaotic regions emerge around an unstable fixed point at $(q, p) = (0, 0)$, and Poincaré-Birkhoff chains induced by nonlinear resonances become visible. Relatively large nonlinear resonances in the inner torus region, which represents librational motions in the pendulum Hamiltonian H , are $1:8$, $1:10$, and $1:12$ ones, which are marked in dark blue in Fig. 1(b). Below we mainly develop our discussion in the case $\tau = 1$, but essentially the same argument follows for other τ cases.

We numerically solve the eigenvalue problem for the unitary operator \hat{U}

$$\hat{U}|\Psi_n\rangle = u_n|\Psi_n\rangle, \quad (3)$$

under the periodic boundary condition on the region $(q, p) \in (-1, 1] \times (-1/2\tau, 1/2\tau]$. Let N be the dimension of the Hilbert space space, then to achieve the periodic boundary condition the relation $1/2\tau \times 2/h = 2\pi N$ should hold, which yields the relation $h = 2/N\tau$.

Here u_n is expressed as $u_n = e^{-iE_n\tau/h}$ where E_n ($n = 0, 1, 2, \dots$) are quasi-energies, and $|\Psi_n\rangle$ denote the corresponding quasi-eigenstates. Hereafter we focus on the doublet states in bounded states supported by the inner torus region, each of which is centered at $(q, p) = (\pm 1/2, 0)$ and energy splittings between them.

Quasi-eigenstates $|\Psi_n\rangle$ have a symmetry with respect to the mirror transformation $\hat{\Pi}_q : q \mapsto -q$, and we hereafter denote the doublet states associated with this symmetry by $|\Psi_n^\pm\rangle$ and the corresponding quasi-energies by E_n^\pm , which form quasi degeneracy. We therefore assign the quantum number n not to an individual quasi-eigenstate but to each doublet [23]. The states $|\Psi_n^+\rangle$ and $|\Psi_n^-\rangle$ respectively represent symmetric and anti-symmetric states. Note that we have additional symmetry with respect to the translation $\hat{T}_1 : q \mapsto q + 1$, originating from the periodic boundary condition in the q -direction. This symmetry does not induce quasi degeneracy in energy, but the states belonging to a different translational symmetry class do not interact with each other even if they have the same mirror symmetry.

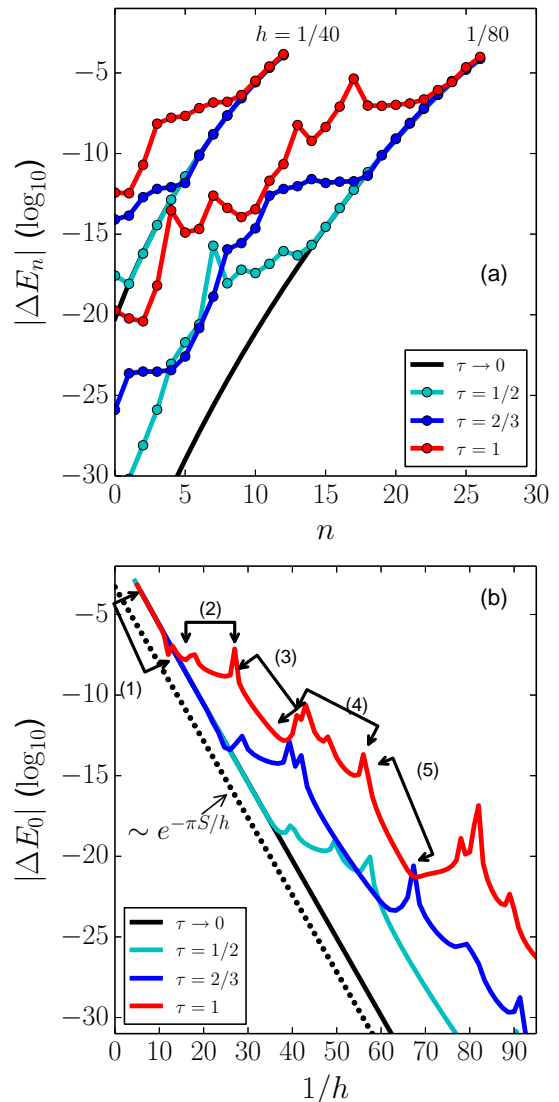


FIG. 2: (Color online) (a) The tunneling splitting ΔE_n is plotted as a function of the quantum number n , where n is labeled not for an individual state but for a doublet (see the text). The value of h for each curve is put in the figure. The black curves represent the splitting $\Delta E_n^{(1)}$ in the limit ($\tau \rightarrow 0$) (b) The tunneling splitting ΔE_0 for the lowest doublet $|\Psi_0^\pm\rangle$ is shown as a function of $1/h$. The black solid and dotted curves correspond to the splitting $\Delta E_0^{(1)}$ in the limit ($\tau \rightarrow 0$) and the semiclassical prediction (1), respectively. In (b), we put the labels (1), (2), \dots , (5) on each characteristic interval: (1) first exponential decay (instanton), (2) first plateau, (3) second steeply decay, (4) second plateau, and (5) third steeply decay regime, respectively.

In the continuous limit $\tau \rightarrow 0$, the eigenvalue equation for the Hamiltonian $H(q, p) = p^2/2 + V(q)$ is expressed as

$$\hat{H}(\hat{q}, \hat{p})|J_n^\pm\rangle = E_n^{\pm, (1)}|J_n^\pm\rangle, \quad (4)$$

where eigenstates $|J_n^\pm\rangle$ are in the same symmetry class

as the corresponding $|\Psi_n^\pm\rangle$. Here the quantum number n is, as usual, attached in ascending order of eigenvalue $E_n^{\pm,(1)}$, so $|J_n^\pm\rangle$ represents the ground state doublet, which we will hereafter focus on.

For the later purpose, we rearrange the quantum number n for the quasi eigenstates $|\Psi_n^\pm\rangle$ such that the overlap $|\langle J_n^\pm|\Psi_n^\pm\rangle|^2$ is maximal. This condition, that is one-to-one correspondence between $|\Psi_n^\pm\rangle$ and $|J_n^\pm\rangle$ is fulfilled for the values of τ used in the present analysis.

With increase in the value of $1/h$, the tunneling probability between $|\Psi_n^\pm\rangle$, which could be measured by the tunneling splitting $\Delta E_n = E_n^+ - E_n^-$, becomes large in several orders of magnitude as compared to those predicted in the continuous limit. The latter is evaluated as $\Delta E_n^{(1)} = E_n^{+, (1)} - E_n^{-, (1)}$. We notice that the overall behavior does not depend on the value of the perturbation strength τ , although the Planck's cell can resolve chaotic regions and nonlinear island chains in the case of $\tau = 1$, whereas this does not the case at all for $\tau = 2/3$. (see Fig. 1 and Fig. 3).

We illustrate such anomalous enhancement of tunneling probability in a nearly integrable regime in two ways. First, as shown in Fig. 2(a), the tunneling splitting ΔE_n is plotted as a function of the quantum number n , and in Fig. 2(b) the splitting ΔE_0 as a function of $1/h$. The latter is known to be a standard plot often used in the study of RAT [8–12].

In Fig. 2(a) we notice that, in the relatively large n regime, ΔE_n can be fitted by the lines predicted by the formula (1), implying that they have completely integrable nature in essence. On the other hand, as n goes down from excited states to the ground state, with a fixed \hbar , the law described by the formula (1) is violated at certain critical quantum numbers n_c , each of which depends on the value of h [8, 21].

At such a quantum number n_c , the curve for ΔE_n changes its slope and forms the plateau. After a certain plateau interval, as typically seen in $\tau = 1$ and $\tau = 2/3$ for $h = 1/80$, the slope again becomes large, and then forms the second plateau. The emergence of plateaus means the enhancement of the tunneling probability as compared to the integrable (instanton) prediction. It is particularly non-trivial and even paradoxical because this enhancement is relatively stronger in the lower doublets than higher excited ones. Note also that the critical quantum number n_c becomes large with increase in the value of τ . This sudden departure from integrable tunneling has been pointed out in the study of RAT [8], and it is called the *instanton-noninstanton* (I-NI) transition in Ref. [20, 21], in which the mechanism behind it has been investigated in a different perspective.

The I-NI transition is similarly observed in the ΔE_n vs $1/h$ plot. As shown in Fig. 2(b), the energy splitting ΔE_0 for the lowest doublet $|\Psi_0^\pm\rangle$ exhibits a similar behavior. For relatively large values of h , ΔE_0 follows the instanton prediction Eq. (1), but deviates from it at certain values of h , each of which depends on the value of τ . The staircase-like structure formed with plateau and

steeply decaying intervals again characterize the overall structure. For the purpose of illustration, we call each region in the staircase, (1) first exponential decay (instanton) (2) first plateau, (3) second steeply decay, (4) second plateau, and (5) third steeply decay regime, respectively (see Fig. 2(b)).

What is prominent in the latter plot than in the former plot is the appearance of spikes. This is because in the former plot Fig. 2(a), we could evaluate tunneling splitting only at integer values (quantum numbers), so may miss spikes even if they exist, whereas we can scan ΔE_0 at more numerous values of $1/h$.

The origin of spikes is a central issue in theory of RAT [9, 11, 12], in which the effect of nonlinear resonance is incorporated by first constructing local integrable pendulum Hamiltonian classically and then applying quantum perturbation theory. Plotting the energy levels as a function of some parameter, k for example, one can recognize that the mechanism of the enhancement due to RAT is similar to CAT: as the parameter is varied, the states forming the reference doublet, $|\Psi_0^\pm\rangle$ in the present case, come close to a third state. They interact with each other, and in the interaction regime the splitting between the reference doublet becomes large, resulting in a spike [12]. Note, however, that the staircase structure formed with the plateau and steeply decaying regime has never been found at least in the completely integrable systems studied so far.

III. STAIRCASE STRUCTURE WITH RESONANCE SPIKES

A. Resonance spikes and the third states

Each spike observed in Fig. 2(b) appears as a result of energy resonance between the doublet $|\Psi_0^\pm\rangle$ and a certain third state. The spikes mostly appear in the plateau regime, but sometimes they are situated in the steeply decaying regime. In Fig. 3, we first demonstrate which type of third states are actually involved in the creation of spikes. In the original framework of the RAT theory, the predicted spikes are associated with the states supported by nonlinear resonances in the inner torus region, encircling central elliptic fixed points, $(q, p) = (\pm 1/2, 0)$ in the present case. However, two of spikes in the first plateau appear as a result of resonance with the states associated with an outer transversal torus and the spike located at the end of the first plateau $h = 1/27$ is associated with the state localized on the unstable fixed points $(q, p) = (0, 0)$ and $(-1, 0)$ (see Fig. 3(b)). This is not surprising since the present eigenstates are Floquet states, so the eigenphase $\tau E_n/\hbar$ of Eq. (3) can satisfy the resonance conditions $E_n - E_\ell = mh/\tau$ ($n, \ell, m \in \mathbb{Z}$). Therefore the quasi-energies of our reference doublet can resonate with a state associated with an outer transversal torus. Such situations are out of the scope of the theory of RAT, but as will closely be discussed in section IV,

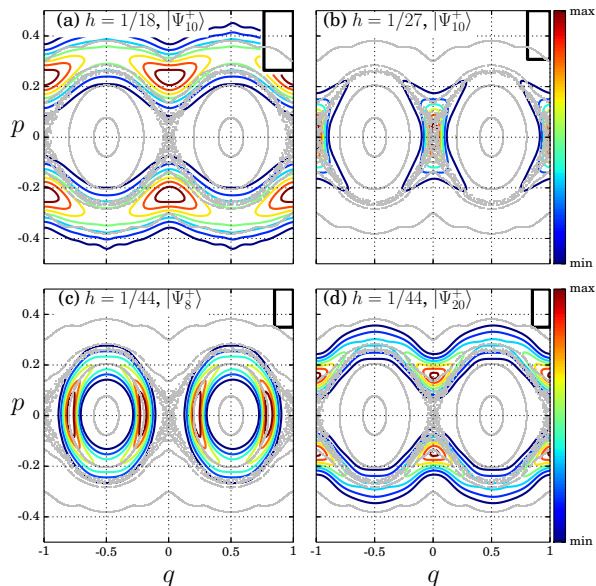


FIG. 3: (Color online) Husimi representation of the third states for $\tau = 1$, which resonantly interact with the reference doublet in the first plateau regime: (a) $1/h = 18$ (at the middle of the first plateau), (b) $h = 1/27$ (at the end of first plateau), (c) and (d) $h = 1/44$ (at the second plateau regime). In (a), (c) and (d) we only show $|\Psi_n^+\rangle$ states out of each tunneling doublet. In (b), the state $|\Psi_n^+\rangle$ is not the one forming a doublet as mentioned in [23]. Upper left box represents the size of effective Planck's cell.

the outer torus states play a crucial role in the formation mechanism of the staircase structure.

Figures 4(a) and (b) demonstrate the splitting ΔE_0 (in the back panel), together with the behavior of doublet and the third state energies (in the floor panel) as a function of the parameter k . When a spike appears in the ΔE_0 vs $1/h$ plot, there always exist spikes in the plot of ΔE_0 vs k nearby. However, even if a spike appears in the ΔE_0 vs $1/h$ plot, it does not necessarily mean that one exactly hits a spike in the plot of ΔE_0 vs k . These figures reveal that the third state for $1/h = 27$ (at the end of the first plateau) is the 10-th excited state $|\Psi_{10}^+\rangle$ and this state is, as shown in Fig. 3 (b), localized on the unstable fixed point $(q, p) = (0, 0)$. On the other hand, $1/h = 44$ (in the middle of the second plateau), there appear two spikes in the range under observation, one is the doublet composed of the 8-th excited states $|\Psi_8^\pm\rangle$ whose symmetric state is shown in Fig. 3 (c), and the other is also given as a doublet of excited states, $|\Psi_{20}^\pm\rangle$ whose symmetric state is shown in Fig. 3 (d). As demonstrated in Figs. 3 (c) and (d), both doublets $|\Psi_8^\pm\rangle$ and $|\Psi_{20}^\pm\rangle$ are supported by elliptic inner and transversal outer KAM curves, respectively.

B. Absorbing operator

Since the present situation, the case of $\tau = 1$, is not far from the integrable limit, eigenstates $|J_\ell\rangle$ in the integrable limit well approximate eigenstates $|\Psi_n\rangle$, *i.e.*, $\langle J_\ell | \Psi_n \rangle \approx 1$. On the basis of this observation, we introduce the following absorbing operator [24, 25]

$$\hat{P} = \hat{1} - \frac{\Gamma}{2} \sum_{\ell \in L} |J_\ell\rangle \langle J_\ell|. \quad (5)$$

Here $\Gamma \leq 2$ represents the absorbing strength, and $\hat{1}$ the identity operator. The summation runs over a given index set L , which we choose appropriately depending on which states we want to suppress [34]. Below we consider the right eigenvalue problem for the absorbed (non-unitary) evolution operator

$$\hat{U}^\circ |\tilde{\Psi}_n\rangle = \tilde{u}_n |\tilde{\Psi}_n\rangle, \quad (6)$$

where

$$\hat{U}^\circ = \hat{P} \hat{U}, \quad (7)$$

and $\tilde{u}_n = e^{-i\tilde{E}_n \tau / \hbar}$. The following argument holds even if one considers the left eigenvalue problem.

First we will discuss what we can expect in perturbation theory with respect to the absorbing strength Γ . It is easy to show that a standard perturbative calculation up to the second order provides

$$\tilde{u}_n \simeq u_n \cdot z_n, \quad (8a)$$

where

$$z_n = 1 - \frac{\Gamma}{2} \sum_{\ell \in L} |a_{\ell, n}|^2 + \frac{\Gamma^2}{4} \sum_{\ell \in L} \sum_{m \neq n} \frac{|a_{\ell, n}^* a_{\ell, m}|^2}{u_n - u_m} u_m, \quad (8b)$$

and

$$a_{\ell, n} = \langle J_\ell | \Psi_n \rangle. \quad (8c)$$

The right (absorbed) eigenstate is also given as

$$|\tilde{\Psi}_n\rangle \simeq |\Psi_n\rangle - \frac{\Gamma}{2} \sum_{m \neq n} B_{m, n} |\Psi_m\rangle \quad (9a)$$

$$= |\Psi_n\rangle - \frac{\Gamma}{2} \sum_{k=0}^{N-1} \sum_{m \neq n} B_{m, n} a_{k, m} |J_k\rangle, \quad (9b)$$

where

$$B_{m, n} = \sum_{\ell \in L} \frac{a_{\ell, m}^* a_{\ell, n}}{u_n - u_m} u_m. \quad (9c)$$

For $0 < \Gamma \leq 2$, (absorbed) quasi-energies \tilde{E}_n are no more real because the second-order term in the perturbation expansion Eq. (8b) becomes complex while the

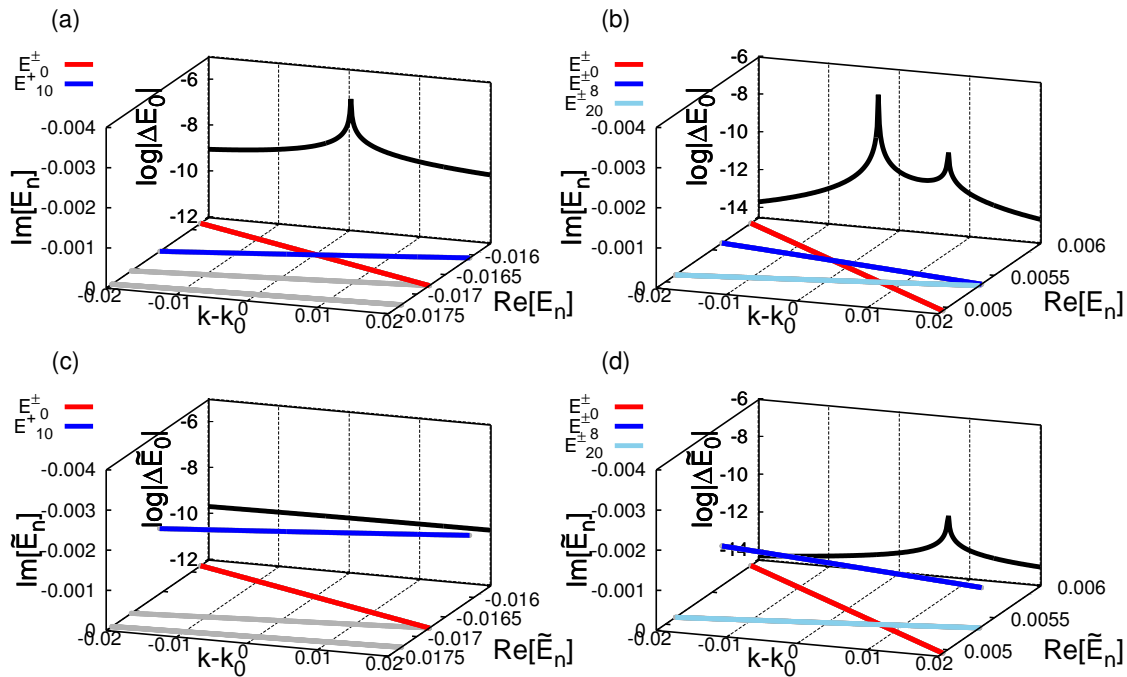


FIG. 4: (Color online) Energy splittings ΔE_0 (black lines in the back panel) and the reference doublet (red lines in the floor panel) and the related third state energies (blue and light blue lines in the floor panel) as a function of the parameter k . For each curve, the corresponding energy level is put in the figures. Gray lines indicate energies of the states irrelevant to creating spikes. In the upper panels, no absorber is applied for (a) $1/h = 27$ and (b) $1/h = 44$. In the lower panels, the strength of the absorber is set as $\Gamma = 1$ for (c) $1/h = 27$ and (d) $1/h = 44$. The index set L is given as (a) $L = \{10\}$ and (b) $L = \{8\}$.

first-order term is real-valued. The eigenvalue \tilde{u}_n is then shifted as

$$\arg \tilde{u}_n = \arg u_n + \arg z_n. \quad (10)$$

By applying the absorber, the coupling between the absorbed and the rest of eigenstates is suppressed. This could be regarded as an inverse procedure of what is done in typical perturbation theory such as RAT theory, in which one starts with some unperturbed states $|J_n\rangle$ and build up desired eigenstates $|\Psi_n\rangle$ by adding perturbation terms. The present absorbing method is, in a sense, to subtract perturbed terms $|J_n\rangle$ from the final state $|\Psi_n\rangle$. Therefore, applying the absorber in this way would be a test to check whether the final state $|\Psi_n\rangle$ could be obtained as a result perturbation in terms of unperturbed states $|J_n\rangle$, and, if so, which unperturbed states are involved in the perturbation procedure. The present absorbing method is equivalent to the one used in the open quantum systems, e.g., [11, 26–28], in which the absorbers are adopted as the Heaviside step function $\langle x|J\rangle = H(x)$ or the Dirac delta function $\langle x|J\rangle = \delta(x)$.

The efficiency of the absorbing method is demonstrated in Figs. 4(c) and (d). For absorbed quasi-energies, the tunnel splitting $\Delta \tilde{E}_n^\pm$ is defined as $\Delta \tilde{E}_n = \tilde{E}_n^- - \tilde{E}_n^+$, however we note that \tilde{E}_n^\pm has an imaginary part when $\Gamma > 0$. Each corresponds to the case where the absorber with $\Gamma = 1$ is applied to the case shown in Fig. 4(c) and (d), respectively. Here the index set L is chosen

as $L = \{10\}$ in the case of $1/h = 27$, and $L = \{8\}$ whose member corresponds to the doublet of the symmetric and anti-symmetric state $|J_8^\pm\rangle$ for $1/h = 44$. Here $\{\ell\}$ represents $|J_\ell^\pm\rangle$, and the member $|J_\ell^\pm\rangle$ in the index set L is chosen in such a way that it maximally overlaps with the third state that is interacting the reference doublet $|\Psi_0^\pm\rangle$ and responsible for creating the spike.

As clearly shown, energies of the associated third states gain certain amount of the imaginary part and pushed out to the complex plane, resulting in vanishing the spikes. The effect to the other states is almost negligible. However, as seen in Fig. 4(d), the right-hand peak with shorter height still remains since we have not include the states $|J_{20}^\pm\rangle$ in the absorber. As mentioned in the end of the previous subsection III A, there are two sets of doublets which are involved in avoided crossings in question.

C. Staircase structure

In the previous subsection, we have selected out absorbing states by plotting energy levels around each avoided crossing and then judging by hand which states should be included in the set L , that is, it was necessary to refer to the figures like Fig. 4. We now introduce a systematic procedure to choose the absorbing states necessary to suppress the observed spikes.

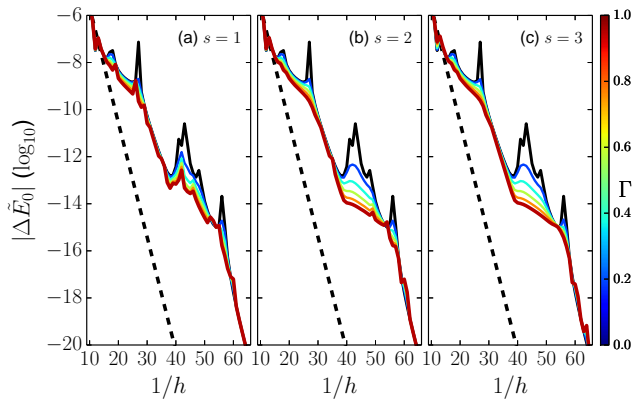


FIG. 5: (Color online) Tunneling splittings $|\Delta\tilde{E}_0|$ for the evolution operator \hat{U}° are plotted as a function of $1/h$. The range of interaction is increased as (a) $s = 1$, (b) $s = 2$, and (c) $s = 3$. Black curves show the unitary case ($\Gamma = 0$) and each colored curve the case with absorber, and the colors distinguish the absorbing strength Γ (see the right-hand color bar). The splitting ΔE_0 in the integrable limit is shown as black dashed lines in each figure.

The most natural criterion to achieve this would be to check the energy difference from the reference doublet: $d(E_n^\pm) = |E_0^\pm - E_n^\pm|$ ($n = 1, 2, \dots$), because the spikes appear when the reference doublet and a certain third state are energetically close to each other and form avoided crossings. We rearrange the states $|\Psi_n^\pm\rangle$ in ascending order of $d(E_n^\pm)$, and the corresponding integrable base $|J_n^\pm\rangle$ as well. The one-to-one correspondence between $|\Psi_n^\pm\rangle$ and $|J_n^\pm\rangle$ is again ensured since the condition $|\langle J_n^\pm | \Psi_n^\pm \rangle| \approx 1$ is now satisfied for $\tau = 1$. Then the set of absorbing states containing the first s doublets in the sense of the energy distance reads

$$L_s = \{1, 2, \dots, s\}, \quad (11)$$

where we drop from the list of L_s the states not belonging to the same parity as $|\Psi_0^\pm\rangle$. We must recall that the ground state $|\Psi_0^\pm\rangle$ has the symmetry with respect to the translation in addition to the mirror transformation.

Note that the set L_s of absorbing states depends on the value of h , so has to be determined for each h . As explained below, the reason why we consider the cases $s > 1$ is that the energetically nearest state L_1 from the reference doublet is not sometimes sufficient for killing the coupling with the reference doublet.

Figure 5 plots the splitting of quasi-energy \tilde{E}_0^\pm evaluated for the operator \hat{U}° as a function of $1/h$. In the $s = 1$ case, we see that some spikes, especially in the first plateau, disappear with increase in Γ . As shown in Fig. 4, the absorber pushes the third level into the complex domain, and the coupling with the reference doublet is suppressed.

However, we notice that some spikes still remain in the second plateau regime. This is due to the fact that, as

shown in Fig. 4(b), some spikes come close to each other in the second plateau and a single absorber is not enough to suppress the interaction with the reference doublet. In the case presented in Fig. 4(b), the third state responsible for the left-hand peak is the state supported by an elliptic torus inside the KAM region and the right-hand one is supported by a transversal torus. As we further add the corresponding absorbers in this way, the peaks surviving in the $s = 2$ case gradually disappear, and the curve almost converges at $s = 2$.

It would be worth emphasizing that steeply decaying regions are not affected and robust against the the absorber applied on plateaus. This strongly suggests that the influence of spikes is well localized in each plateau, not like the situation suggested in [11]. This observation also supports our hypothesis; the splitting curve should be viewed as a staircase structure accompanied by spikes, not as spikes bringing the staircase.

IV. MECHANISM GENERATING THE STAIRCASE STRUCTURE

The main message in the previous section is that the staircase-shaped skeleton is formed in the splitting curves and spikes are superposed on it. In this sense we may say that the origin of the enhancement of the tunneling probability traces back to such a staircase structure. In this section, we study the mechanism creating the staircase structure by introducing the renormalized basis, and show the reason why this only appears in nonintegrable systems.

A. Instanton-noninstanton transition

As shown in [21], the I-NI transition could be well captured by renormalized perturbation theory. An important finding there was that a remarkable quenching of renormalized transition matrix elements explains the I-NI transition. In particular, without using highly renormalized integrable Hamiltonian as unperturbative bases one could not identify the mechanism behind the transition.

For this reason, we also apply the same perturbation scheme to pursue the origin of the staircase structure. In essence, renormalized perturbation theory makes use of the Baker-Campbell-Hausdorff (BCH) expansion [21, 29]:

$$\hat{U} \approx \hat{U}_M \equiv \exp \left[-\frac{i}{\hbar} \tau \hat{H}_{\text{eff}}^{(M)}(\hat{q}, \hat{p}) \right], \quad (12)$$

where

$$\hat{H}_{\text{eff}}^{(M)}(\hat{q}, \hat{p}) = \hat{H}_1(\hat{q}, \hat{p}) + \sum_{\substack{j=3 \\ (j \in \text{odd int.})}}^M \left(\frac{i\tau}{\hbar} \right)^{j-1} \hat{H}_j(\hat{q}, \hat{p}). \quad (13)$$

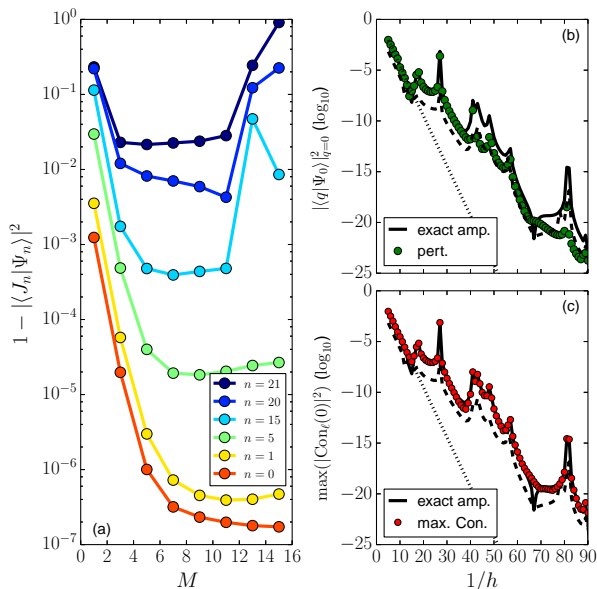


FIG. 6: (Color online) (a) Left panel shows the error $1 - |\langle J_n^{(M)} | \Psi_n \rangle|^2$ as a function of the BCH order M in the case of $h = 1/63$. Not only the grand state, $n = 0$, but also excited states up to $n = 74$ are examined. (b1) The amplitude at $q = 0$ of the ground state obtained by the perturbation calculation, and (b2) the amplitude of the maximal mode of the contribution spectrum (see the text). The exact amplitude for the ground state $|\Psi_0\rangle$ at $q = 0$ is shown as blue curves in (b1) and (b2). The solid black dashed and dotted curves show the exact level splitting ΔE_0 and the level splitting $\Delta E_0^{(M)}$ of the integrable basis for reference, respectively.

Here \hat{H}_j denotes the j -th order term in the BCH series. Explicit forms for the first few terms are found as

$$\hat{H}_1(\hat{q}, \hat{p}) = T(\hat{q}) + V(\hat{p}), \quad (14a)$$

$$\hat{H}_3(\hat{q}, \hat{p}) = \frac{1}{24}([T, [T, V]] - [V, [V, T]]), \quad (14b)$$

⋮

where the terms \hat{H}_j for even j are equal to zero thanks to the symmetrized form of \hat{U} . The first order BCH Hamiltonian $\hat{H}_{\text{eff}}^{(1)}$ is identical to the continuous time Hamiltonian and higher order BCH Hamiltonians $\hat{H}_{\text{eff}}^{(M)}$ are expressed as nested commutators. We denote the eigenfunctions of the integrable Hamiltonian $\hat{H}_{\text{eff}}^{(M)}$ by $|J_\ell^{(M)}\rangle$:

$$\hat{H}_{\text{eff}}^{(M)} |J_\ell^{(M)}\rangle = E_\ell^{(M)} |J_\ell^{(M)}\rangle. \quad (15)$$

We first check the validity and efficiency of renormalized perturbation bases by examining the error $1 - |\langle J_n^{(M)} | \Psi_n \rangle|^2$ of the approximation. As shown in Fig. 6(a), the BCH states becomes better approximation to the corresponding eigenstate $|\Psi_n\rangle$ as the expansion order M increases. Note also that the expansion works for the lower energy eigenstates as compared to the higher

excited states. This is, however, not a convergent expansion: the error $1 - |\langle J_n^{(M)} | \Psi_n \rangle|^2$ starts to grow when the expansion order M exceeds a certain optimal order.

Such highly efficient integrable approximation ensures the validity of renormalized perturbation, in which the difference $\Delta \hat{U}_M = \hat{U} - \hat{U}_M$ could be regarded as a perturbation [21]. As also shown in Fig. 6(b1), the results of the 1st order perturbation calculation are in an excellent agreement with the exact ones, and even the staircase structure could be reproduced. However we would like to remark that although perturbation theory, not necessarily the present one, works well, this does not tell us anything about the underlying mechanism generating the staircase.

As shown in Fig. 6(b1), the splitting ΔE is strongly correlated with the amplitude of the eigenstate at $q = 0$, and characteristic patterns appear around $q = 0$. As seen in Fig. 7(a), the eigenstate $|\Psi_0\rangle$ for $\tau = 1$ in the instanton regime is, as expected, well fitted by the one $|J_0^{(M)}\rangle$ in the integrable bases, whereas the integrable approximation does not work any more and further structures appear in other regions. In the first and second plateau, the curve bends in a convex way (see Fig. 7(b) and (d)), but in the first steeply decaying region the curve bends in a downward direction at $q = 0$ and takes a concave structure (see Fig. 7(c)).

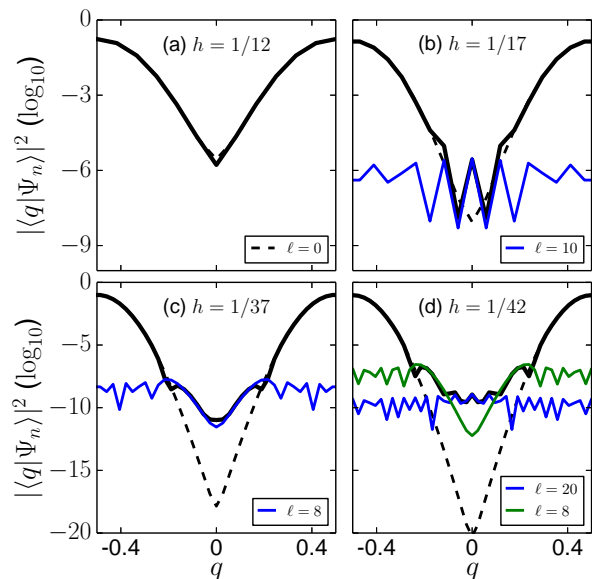


FIG. 7: (Color online) The black curve in each figure shows the eigenstate $|\Psi_0\rangle$ for $\tau = 1$ in the (a) instanton, (b) first plateau, (c) second decay and (d) second plateau regime, respectively. The dashed curve displays the integrable eigenstate $\langle q | J_0^{(M)} \rangle$ at the corresponding h value, and colored ones the integrable components $\langle q | J_\ell^{(M)} \rangle \langle J_\ell^{(M)} | \Psi_0 \rangle$ at $q = 0$, where the value of ℓ is put in each figure. Note that the structure around $q = 0$ can be well reproduced by the maximal mode(s) of the contribution spectrum (see the text).

To explore the nature of wavefunctions at $q = 0$, we here introduce a spectrum decomposition at each position q in terms of integrable bases $|J_\ell^{(M)}\rangle$:

$$\langle q|\Psi_0^+\rangle = \sum_{\ell=0}^{N-1} \text{Con}_\ell^{(M)}(q) \quad (16)$$

where

$$\text{Con}_\ell^{(M)}(q) = \langle q|J_\ell^{(M)}\rangle \langle J_\ell^{(M)}|\Psi_0^+\rangle. \quad (17)$$

We call such a decomposition the *contribution spectrum* [21]. In the following discussion, we focus only on the symmetric ground state $|\Psi_0^+\rangle$. As we mentioned in Sec. II, each eigenstate has a symmetry with respect to the mirror transformation $\hat{\Pi}_q$ and the translation \hat{T}_r . Therefore, the basis $|J_\ell^{(M)}\rangle$ that has the same symmetry as $|\Psi_0^+\rangle$ is only used for the contribution spectrum.

As shown in Fig. 6(b2), since the maximal mode of the contribution spectrum quite efficiently describes the behavior of the splitting, we can deduce that the staircase structure must be characterized by the maximal mode. Indeed, in Ref. [21], we have shown that the instanton-noninstanton (I-NI) transition could be explained as the switching behavior of the most dominant component in the contribution spectrum; from the one representing the instanton contribution to broad components supported around the separatrix of a central unstable fixed point. Below, we present that the dominant component controls not only the transition from instanton to noninstanton but overall signatures in the staircase structure. We will explain this by showing contribution spectra for several values of $1/h$, which are presented in Fig. 8.

First of all, as mentioned just above, we notice that the contribution spectrum is mainly composed of two peaks with distinct characteristics. The first one is a sharp peak located at $E = E_0^{(M)}$, and the second is composed of many components, whose center is situated around the separatrix energy. A small peak sometimes appears on the broadly spread components as a result of the interaction with a third state. The first sharp peak at $E = E_0^{(M)}$ originates from the instanton contribution that has a maximal overlap with the ground state $|\Psi_0^+\rangle$, so we hereafter call it the instanton peak. We stress again that the instanton peak at $E = E_0^{(M)}$ can be recognized only when we prepare higher order BCH expansions ($M = 7$ for the present calculation), otherwise the instanton peak is not isolated from the others and could not be identified.

In the instanton decay (the first steeply decaying) regime, which is seen in the case of $1/h = 12$ in Fig. 8(a), the instanton peak dominates the other components. As a result the amplitude of the ground state $|\Psi_0^+\rangle$ at $q = 0$ is well described by the integrable Hamiltonian base $|J_0^{+, (M)}\rangle$. Hence the instanton behavior should and is actually observed.

With increase in $1/h$, the height of both peaks, the instanton peak and the broad components centered around

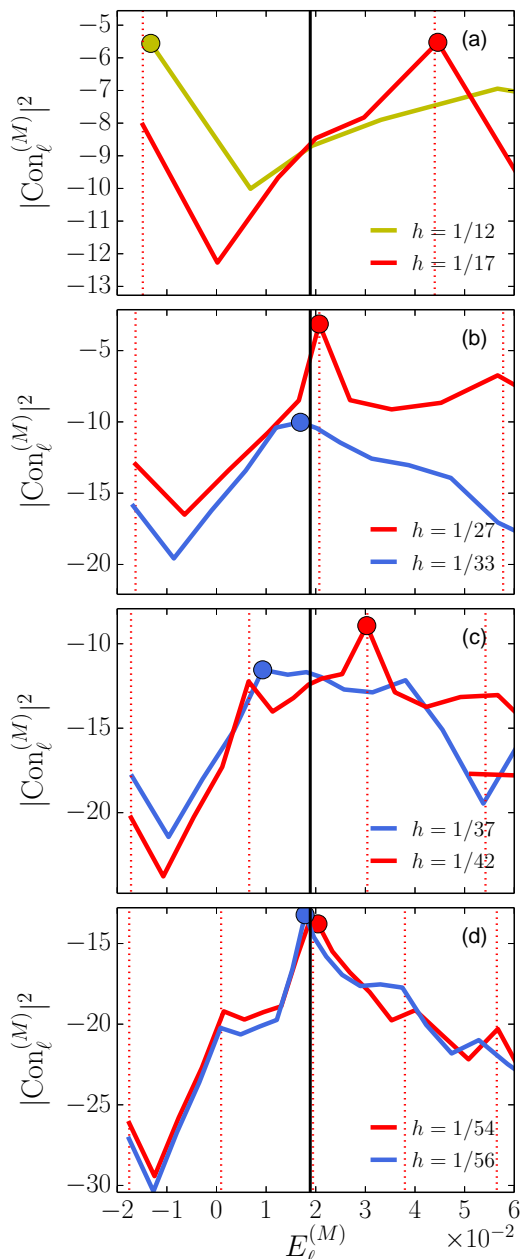


FIG. 8: (Color online) The contribution spectrum $\text{Con}_\ell^{(M)}$ (in \log_{10} scale) at $q = 0$ is plotted as a function of the energy $E_\ell^{(M)}$. The BCH order $M = 7$ was used. The values of h are indicated in each figure. Each panel respectively shows the case (a) before (yellow) and after (red) I-NI transition, (b) before (red) and after (blue) the transition from the first plateau to the second decaying, (c) before (blue) and after (red) the transition from the second decaying to the second plateau, (d) before (red) and after (blue) the transition from the second plateau to third steep decaying regime. The dot represents the maximal mode in each spectrum. We have used a yellow-colored curve in the region where the maximal mode is given by the instanton contribution, a red-colored when the maximal mode energy is above the separatrix energy, and a blue-colored below the separatrix energy. The thick solid line represents the separatrix energy and red dotted lines the energies satisfying the condition $E = E_0^{(M)} + mh/\tau$ ($m = 0, 1, 2, \dots$) (see the discussion in subsection IV B).

the separatrix, gradually drop, but the speed of the former is much higher than that of the latter, eventually resulting in the switching of the role of the dominant contributor from the instanton to the top of broad components. An important remark is that the support of the state associated with the top of the broad components is outside the separatrix, meaning that the ground state is most dominantly coupled with an outside state [21]. We notice in Fig. 6(b) that, exactly at this switching moment, the first instanton decay turns to the first plateau, and eigenstates show the convex structure around $q = 0$ (see Fig. 7(b)). In the perturbation calculation, it is also crucial to include outer torus states into unperturbed bases to reproduce the convex structure at $q = 0$, otherwise the resulting wavefunction cannot bend upward at $q = 0$ since it is merely a superposition of exponentially decaying states. It is important to note that not only such a convex structure just after the transition but also neighboring structures around $q = 0$ could be well reproduced only by the maximal mode in the spectrum $\text{Con}_\ell^{(M)}$ (see Fig. 6(b2)).

In any case, the maximal mode in the spectrum $\text{Con}_\ell^{(M)}$ can be a good indicator for the value of eigenstates at $q = 0$ and thereby the splitting ΔE . The maximal mode in the contribution spectrum $\text{Con}_\ell^{(M)}$, which is shown using color-coded dots in the Fig. 9, well traces the staircase structure of the exact splitting ΔE_n , and the value of eigenstates $|\langle q|\Psi_n\rangle|_{q=0}^2$ at $q = 0$ as well. We will fully make use of this fact hereafter.

As we further increase in $1/h$, the instanton peak is completely overtaken by the broadly spread components (see Fig. 8(b)) and this ordering is fixed and never turned over. We also emphasize that the estimation of the critical Planck's constant h_c at which the I-NI transition occurs becomes a bit imprecise if we use the lower order BCH series.

As we increase $1/h$ after the I-NI transition, the support for the maximal mode of the contribution spectrum further approaches the separatrix, which is shown as in Fig. 8(b), and eventually it goes into the inner tours region in excess of the separatrix. At this moment, we realize that the splitting curve changes the behavior from the first plateau to the second steeply decaying regime (see Fig. 6(b)). At the same time, the structure of eigenstates at $q = 0$ changes from the convex to concave shape (see Fig. 7(c)).

With further increase in $1/h$ the maximal mode also shifts to the left. On the other hand, another peak is born at the right-hand edge of broad components, and now the competition comes into issue between the those peaks, the one playing a major role in the I-NI transition, and the new one at the right-hand edge. As noticed in Fig. 8(c), the switching of the dominant contributor again takes place between these two peaks, and at this moment the splitting curve turns from the second steeply decaying to the the second plateau regime.

After such a transition, the overtaken peak, the one playing a role in the I-NI transition, is gradually ab-

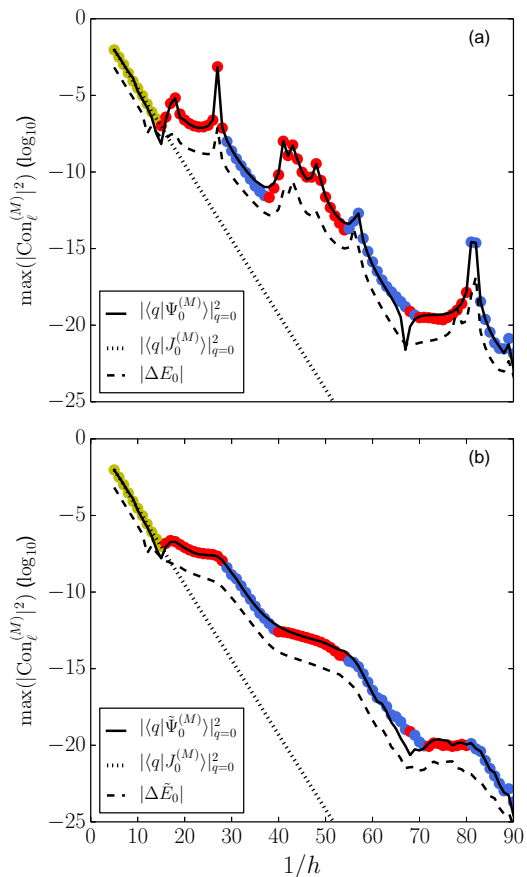


FIG. 9: (Color online) (a) Maximal modes plotted as a function of the inverse Planck's constant $1/h$. We have used yellow-colored dots in the region where the maximal mode is given by the instanton contribution, red-colored ones when the maximal mode energy is above the separatrix energy, and blue-colored below the separatrix energy. (b) Maximal modes for the absorbed eigenstates $|\Psi_n\rangle$. The absorption procedure is the same as that introduced in section III. Here we use the integrable bases $|J_\ell^{(M)}\rangle$ as the absorber, and the absorption parameters are chosen as $s = 3$ and $\Gamma = 0.4$. The rule for color coding is the same as in (a). In both calculations, the BCH order $M = 7$ was used. In (a) the exact eigenfunction $\langle q|\Psi_0^+\rangle$ at $q = 0$, integrable basis $\langle q|J_n^{(M)}\rangle$, and energy splitting ΔE_0 are shown as solid, dotted and broken curves, respectively. In (b) the solid curve represents the absorbed eigenfunction $\langle q|\Psi_0^+\rangle$ at $q = 0$, and dotted and broken ones are the same as in (a).

sorbed into the spectrum envelope. However it leaves a clear trace in wavefunction: As shown in Fig. 7(d), the shoulder or bulge observed in the neighboring region around $q = 0$ is well reproduced by the component that has played a role in the I-NI transition. The convex structure observed in the first plateau is pushed outward by the newly born component, and then it appears as shoulders. In other words, the history of the staircase structure in the splitting plot is properly recorded in the tail of wavefunction, not necessarily at $q = 0$.

The staircase structure in the splitting plot could therefore be explained by the successive switching process of maximal modes, and passing through the separatrix, that is, whether the support of the maximal mode is inside or outside the separatrix. Figure 9 illustrates that the staircase structure of the splitting curve can be understood by the position of the maximal mode: whether its support is outside or inside the separatrix.

We have verified, as shown in Fig. 9(b), that even if we suppress the peak standing on the broad peak components using the same absorber technique in subsection III B, this switching process still survive. This implies that the switching does not occur specifically between the resonance peaks appearing in the contribution spectrum, but overall deformation of broad peak components controls it. We could identify at least the third and fourth transition and confirmed the same scenario applies.

B. Anomaly of eigenfunctions in the action representation

As shown above, we could attribute the emergence of the staircase structure to the successive switching of the dominant component in the contribution spectrum. In this subsection, we explain why the quantum number of the dominant component gradually shifts with increase in $1/h$, passing through the separatrix, and also explain why this causes the change in the slope of the splitting curve.

For this purpose, we examine the behavior of the expansion coefficient $\langle J_\ell^{(M)} | \Psi_0 \rangle$ and the integrable eigenfunction $\langle q | J_\ell^{(M)} \rangle$ at $q = 0$ separately. Note that the product of these two terms constitutes each component in the contribution spectrum $\text{Con}_\ell^{(M)}$. We here call $\langle J_\ell^{(M)} | \Psi_0 \rangle$ the eigenfunction in the action representation.

First of all we remark that the value h/τ becomes a fundamental energy unit in our system. This is because the present system is driven by the periodic force with period τ , so $2\pi/\tau \times \hbar = h/\tau$ becomes a fundamental energy unit, and the energies specified as $E_\ell^{(M)} = E_0^{(M)} + mh/\tau$ ($m = 0, 1, 2, \dots$) may invoke quantum mechanical resonances. In Fig. 8, we have shown such energies as dotted red lines. In the following, we first describe a signature of $\langle q | J_\ell^{(M)} \rangle$ at $q = 0$ and then discuss anomaly found in $\langle J_\ell^{(M)} | \Psi_0 \rangle$. Combining these, we finally explain the mechanism of successive switching in the contribution spectrum.

As shown in Fig. 10, the amplitude of the integrable eigenfunction $\langle q | J_\ell^{(M)} \rangle$ at $q = 0$ shows exponential dependence on the energy $E_\ell^{(M)}$ as far as the energy is less than that of the separatrix (left side of the thick black line in Fig. 10). When plotting $\langle q | J_\ell^{(M)} \rangle$ with a fixed energy one also finds exponential decay as a function of $1/h$ (see Fig. 9(b)). This is an expected behavior since $\langle q | J_\ell^{(M)} \rangle$ is just an eigenfunction of an integrable Hamiltonian, no

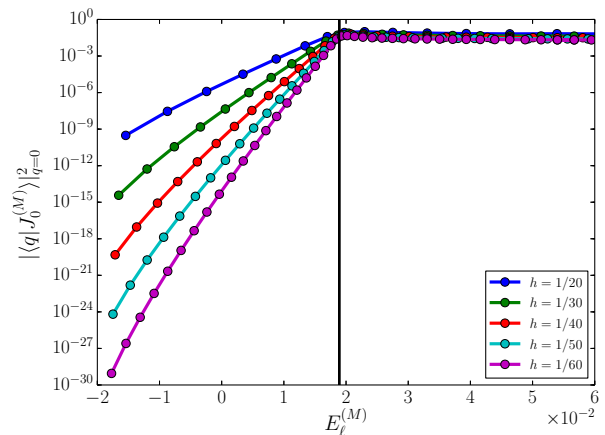


FIG. 10: (Color online) Amplitude of the integrable eigenfunction $\langle q | J_\ell^{(M)} \rangle$ at $q = 0$. The 7th order BCH Hamiltonian was used. The black vertical line shows the energy of separatrix.

matter large the expansion order M is.

On the other hand, above the separatrix energy (right side of the thick black line), we see that the amplitude of the integrable eigenfunction $\langle q | J_\ell^{(M)} \rangle$ keeps almost constant. This is also reasonable because each $\langle q | J_\ell^{(M)} \rangle$ has its supports on a transversal invariant torus outside the separatrix, so the connection is not made via tunneling but real classical processes, thus resulting in no decay as a function of the energy.

In contrast, the nature of the eigenfunction $\langle J_\ell^{(M)} | \Psi_0 \rangle$ in the action representation is highly nontrivial. As shown in Fig. 11(a), there exists a sharp peak at $E_0^{(M)}$, which represents the instanton contribution, and then the value of $\langle J_\ell^{(M)} | \Psi_0 \rangle$ suddenly drops to reach a small level. Then it forms a *non-decaying region* in which the value of $\langle J_\ell^{(M)} | \Psi_0 \rangle$ does not decrease, rather increases gradually until a small peak which is close to the energy which is specified by the relation $E = E_0^{(M)} + h/\tau$ [30, 32]. This peak originates from the resonance of the associated states with the periodic forcing inherent in our model. The non-decaying region means that as long as the eigenphase difference is less than h/τ the contribution from the associated integrable basis states is almost equal. It is beyond this resonance that the exponential decay common in the ordinary tunneling tail takes place. As presented in Figs. 11(b)-(c), the presence of non-decaying region is not limited to the ground state but appears in excited states as well. Also note that overall features are reproduced by just one-step time evolved wavefunction which is expressed as $\langle J_\ell^{(M)} | \Delta U_M | J_n^{(M)} \rangle$. The latter is consistent with the observation that perturbation theory based on the BCH basis works well (see Fig. 6(b)). We emphasize that these are all observed only when the order M of the BCH approximation is large enough and also universally appear in the eigen-

function of quantum maps [21, 30, 32].

A particularly important fact is, as shown in Fig 12, that the decay rate of the height of the non-decaying region as a function of $1/h$ is extremely slow, as compared to the region $E_\ell^{(M)} > h/\tau$. This clearly distinguishes and characterizes the two regions, below and above the resonance energy $E = E_0^{(M)} + h/\tau$. We should make clear the underlying reason behind the observed power law decay in both regions, but the observed energy, so the corresponding classical structure as well, moves with increase in $1/h$ in the current setting, which makes difficult to apply a straightforward semiclassical argument.

In addition to the resonance peak at $E = E_0^{(M)} + h/\tau$, a sequence of peaks implying the higher order resonances appear at $E = E_0^{(M)} + mh/\tau$ (m integer) (see Fig. 11(a)). In conjunction with resonance peaks, there also exist narrow non-decaying regions just below each peak as the non-decaying region appearing in the region $E - E_0^{(M)} < h/\tau$. Such a sequence of non-decaying region is not so sharply identified in Fig. 11(a), but it becomes clearly visible as we increase $1/h$. We can therefore divide each sector $E_0^{(M)} + mh/\tau < E < E_0^{(M)} + (m+1)h/\tau$ into two characteristic regions; the one showing faster decay with $1/h$ and the other having quite slow decaying character. A detailed explanation will be presented in our forthcoming paper [32], and we just show in Fig. 12 the difference of the decay rate by measuring it in the middle energy in each sector. As is seen, the decay rate in the region $E_0^{(M)} + h/\tau < E < E_0^{(M)} + 2h/\tau$ is much slower than in the next sector $E_0^{(M)} + 2h/\tau < E < E_0^{(M)} + 3h/\tau$. Although we do not specify in which characteristic region the middle point energies used to measure the decay rate is contained, it is enough, in the following argument, to notice that the decay rate much differs in each sector. Also note that such resonance peaks with the same nature also appear in excited states as also shown in Fig. 11(b)-(c).

Putting all the pieces together, we can now understand why successive switching in the contribution spectrum generates the staircase structure. In the first decaying (instanton) region, the instanton is the most dominant and broadly spread components provide only negligible contributions, as explained in the previous subsection. The height of the instanton peak decays exponentially with $1/h$ as expected. However, in this region, the largest component in the broadly spread components is outside the separatrix (see the yellow curve in Fig. 10(a)), meaning that the separatrix energy is contained in the non decaying region of $\langle J_\ell^{(M)} | \Psi_0 \rangle$. Since $\langle q | J_\ell^{(M)} \rangle$ keeps constant when the position q is outside the separatrix and the decaying speed of $\langle J_\ell^{(M)} | \Psi_0 \rangle$ is so slow as shown in Fig. 12, its product $\text{Con}_\ell^{(M)}$ also decays much slower than the instanton peak. Thus, at a certain critical $1/h_c$, the instanton component is overtaken by the dominant component in the broadly spread components. This is nothing but the I-NI transition [21].

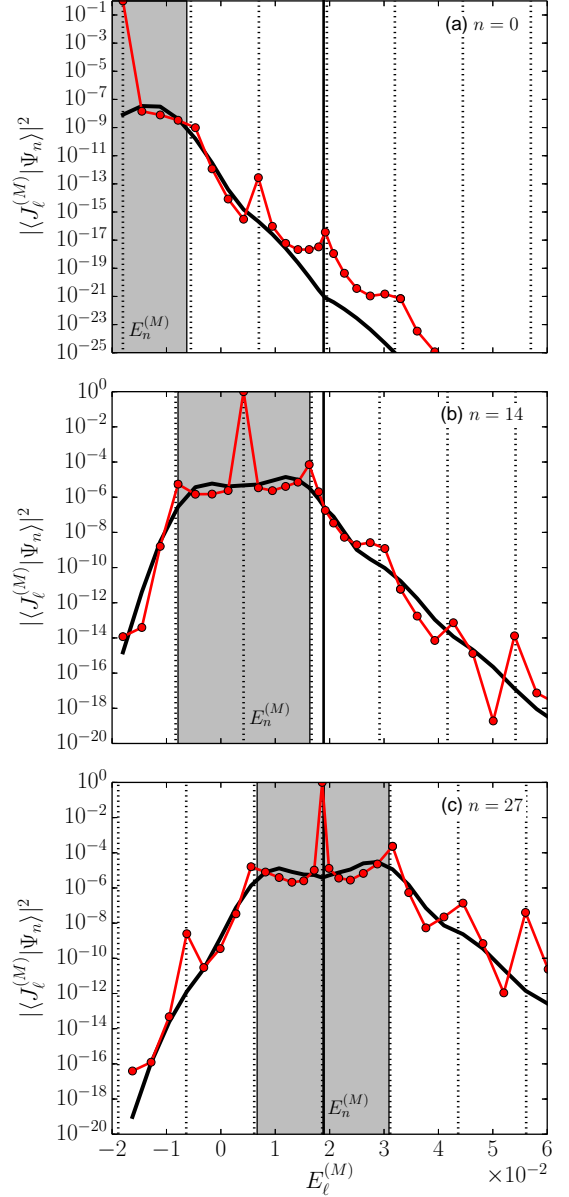


FIG. 11: (Color online) Eigenstates $\langle J_\ell^{(M)} | \Psi_n \rangle$ in the action representation plotted as a function of $E_\ell^{(M)}$ for $h = 1/80$ for (a) $n = 10$, (b) $n = 15$ and (c) $n = 25$, respectively. The black curves show the matrix elements $\langle J_\ell^{(M)} | \Delta \hat{U} | J_n^{(M)} \rangle$. Here we used the 7-th order BCH Hamiltonian as the basis $|J_\ell^{(M)}\rangle$. The black solid line and dotted lines respectively show the separatrix energy, and the energies satisfying the condition $E = E_0^{(M)} + mh/\tau$ ($m = 0, 1, 2, \dots$).

After the I-NI transition, as long as the position of the dominant contribution in the broadly spread components is outside the separatrix, the decaying behavior in the plateau of $\langle J_\ell^{(M)} | \Psi_0 \rangle$ controls the product $\langle q | J_\ell^{(M)} \rangle \langle J_\ell^{(M)} | \Psi_0 \rangle$. This explains the presence of plateau in the splitting curve.

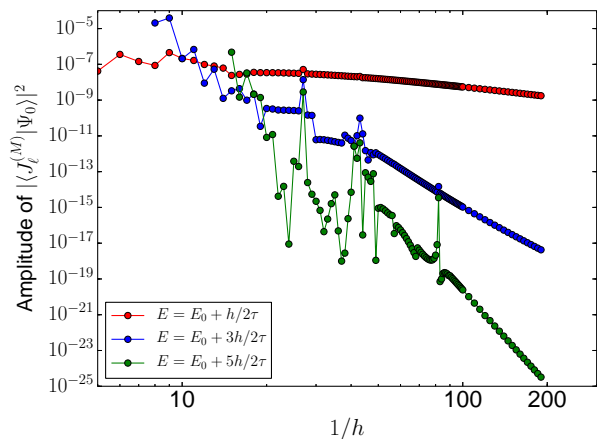


FIG. 12: (Color online) The inverse Planck's constant $1/h$ dependence of $\langle J_\ell^{(M)} | \Psi_0 \rangle$. Difference of colors distinguishes the energy at which the value of $\langle J_\ell^{(M)} | \Psi_0 \rangle$ is evaluated (see the inner panel).

However, note that the position of the dominant component is determined by the edge of the plateau of $\langle J_\ell^{(M)} | \Psi_0 \rangle$, and this edge is located around the value h/τ . As a result, at a certain value of $1/h$, the position of the dominant contribution passes through the separatrix (see Fig. 8(b)). If such an event occurs, the separatrix energy is then situated in the region where $\langle J_\ell^{(M)} | \Psi_0 \rangle$ shows faster decay. This is exactly the moment when the splitting curve turns from the first plateau to the second steeply decaying region.

The mechanism generating the next plateau is understood by observing $\langle J_\ell^{(M)} | \Psi_0 \rangle$ in a wider range. As shown in Fig. 11(a), a sequence of peaks appears at integer multiples of the fundamental energy unit h/τ , and the decay rate of $\langle J_\ell^{(M)} | \Psi_0 \rangle$ just below each resonance peak is again very slow as compared in the next sector, as demonstrated in Fig. 12. Hence the same switching process takes place repeatedly. We have actually checked that the mechanism explained here works at least until the third plateau, but we expect that this continues in larger $1/h$ regimes.

In this way, we could explain the emergence of the staircase structure based on the nature of the action representation, which seems to be closely connected with the fundamental energy sequence whose unit is given as h/τ . As was checked above, the fundamental energy sequence can induce quantum resonances, resulting in the spikes in the splitting curve. However, it should be noted that the appearance of quantum resonances is not a necessary condition for the presence of the staircase structure, as discussed in the subsection III C and IV A. In other words, even if the resonance condition is not satisfied, a broadly spread or mild peak, whose width is almost comparable to the fundamental energy unit h/τ , survives around the fundamental energy sequence. This is quite

an anomalous situation because such a broad peak implies the existence of periodic oscillation of period τ accompanied by a rapid decaying process whose life time is comparable to the oscillation period itself [30].

We also characterize this anomaly from the viewpoint of semiclassical theory. If the leading-order semiclassical approximation works, the matrix element $\langle J_\ell^{(M)} | \Delta \hat{U}_M | J_0^{(M)} \rangle$ should take a form of $\Psi \sim \sum_\gamma A_\gamma e^{-iS_\gamma/\hbar}$, where A_γ and S_γ respectively stand for the amplitude and classical action, and the sum γ is taken over complex classical orbits satisfying given initial and final conditions. In the semiclassical regime, we may neglect the \hbar dependence in the amplitude A_γ , so the matrix element $\langle J_\ell^{(M)} | \Delta \hat{U}_M | J_0^{(M)} \rangle$ is approximately expressed using the minimum imaginary action $\text{Im} S_{\gamma_0}$ as $\Psi \sim e^{-\text{Im} S_{\gamma_0}/\hbar}$. Since $\text{Im} S_{\gamma_0}$ is a purely classical quantity, the form $\hbar \ln \langle J_\ell^{(M)} | \Delta \hat{U}_M | J_0^{(M)} \rangle$ should not depend on \hbar . As will be shown in Fig. 16, this is indeed the case in the integrable system. On the other hand, Fig. 13 shows that the matrix element $\langle J_\ell^{(M)} | \Delta \hat{U}_M | J_0^{(M)} \rangle$ does not follow the semiclassical ansatz in the non-decaying region, whereas the leading-order semiclassical prediction seems to work well beyond the non-decaying region. Although it is necessary to check whether or not the leading-order semiclassical approximation indeed breaks in the non-decaying region, the observed sharp distinction would be an important signature characterizing anomaly.

According to these speculations, we are currently taking two approaches to understand what was observed in the eigenstate $\langle J_\ell^{(M)} | \Psi_0 \rangle$ in the action representation; one is a real semiclassical analysis which is based on the so-called classical-quantum correspondence principle. This could extract anomalous components hidden in classical dynamics generated by the BCH Hamiltonian, and actually reproduce anomalous decay tails [30]. Another approach is to take into account higher-order effects in the semiclassical analysis. Since similar non-decaying or anomalous behaviors have been found in the model with discontinuity in phase space, observed phenomena might be linked to or have at least close similarity with diffraction [31]. This naturally leads us to the semiclassical treatment beyond the leading order. In any case, these are out of the scope of the present paper, and will be reported closely in our forthcoming paper [32].

V. SPLITTING CURVES IN INTEGRABLE SYSTEMS

In the previous subsection, we discussed the underlying mechanism controlling the staircase structure of the splitting curve and found that anomalous tails in eigenfunctions in the action representation play a key role. If such a feature is shared only in nonintegrable maps, we would not expect the enhancement of the tunneling probability in the completely integrable system. Below

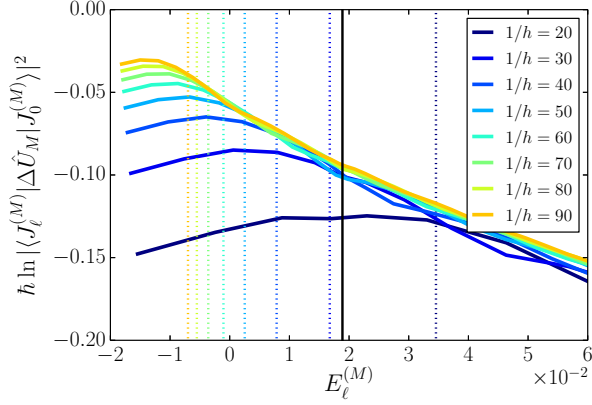


FIG. 13: (Color online) Scaled wavefunction $\hbar \ln |\langle J_\ell^{(M)} | \Delta \hat{U}_M | J_0^{(M)} \rangle|^2$ as a function of $E_\ell^{(M)}$ for several effective Planck's constant h . The black solid line and dotted lines respectively show the separatrix energy, and the energies satisfying the condition $E = E_0^{(M)} + h/\tau$

we shall explain, the nature of the splitting curve in the integrable system is totally different, although a seemingly common behavior is observed.

For this purpose, let us consider the following classically integrable Hamiltonian

$$H(q, p) = H_0(q, p) + \varepsilon H_1(q, p) \quad (18)$$

with

$$H_0(q, p) = (\cos^2 q + \cos^2 p)/2 + a(\cos^2 q + \cos^2 p)^2, \quad (19a)$$

$$H_1(q, p) = \cos^4 p - 6 \cos^2 p \cos^2 q + \cos^4 q. \quad (19b)$$

This system was analyzed in [19] to examine the validity of RAT theory in a completely integrable situation. The authors have introduced a parameter ϕ which controls the relative orientation of the classical resonance chains [19]. Since the formulation of RAT theory do not take into account such orientation, RAT calculation could not follow the difference originating from it [19].

As is seen from the Figs. 14(a1) and (a2), the equi-energy surface has a local maximum between an unstable fixed point $(q, p) = (0, 0)$ and a stable fixed point $(q, p) = (\pm\pi/2, 0)$. Some equi-energy surfaces in the inner well, which appear around the stable fixed points $(q, p) = (\pm\pi/2, 0)$, have the same energies as those in the outer region. For $\varepsilon > 0$, a classical nonlinear resonance chain is developed along the ridge between the inner well and outer region.

We impose the periodic boundary condition on the region $(q, p) \in (-\pi, \pi] \times (0, \pi]$, and solve the eigenvalue problem

$$\hat{H}(\hat{q}, \hat{p})|\Psi_n^\pm\rangle = E_n^\pm|\Psi_n^\pm\rangle. \quad (20)$$

We then consider the splitting $\Delta E_0 = E_0^+ - E_0^-$ of the ground and first excited states, both localizing in the inner

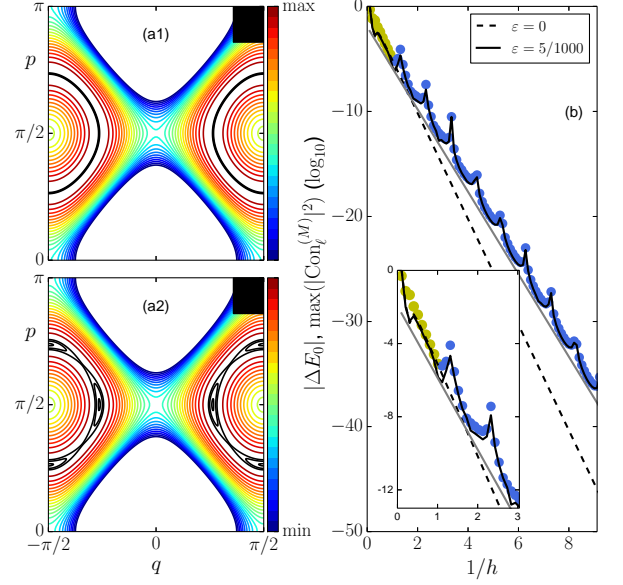


FIG. 14: (Color online) Phase space portrait for the Hamiltonian (18) for $a = -0.55$ and (a1) $\varepsilon = 0$ and (a2) $\varepsilon = 5/1000$. The black curves show the energy contour whose energy value is close to the maximum one. The black box put in the upper right corner represents the size of effective Planck's constant for $h = 1/5$. (b) The splitting ΔE_0 (in \log_{10} scale) as a function of $1/h$ in the cases of $\varepsilon = 0$ (black dashed line) and $\varepsilon = 5/1000$ (black solid line). Yellow and blue dots represent the maximal mode of the contribution spectrum $\text{Con}_\ell^{(M)}$ at $q = 0$ for $\ell = 0$ and for $0 < \ell/N < 1/2$, respectively. The gray line shows the slope of the splitting curve for $\varepsilon = 5/1000$. The inset is magnification of a small $1/h$ regime.

well. Here we take the innermost state in the inner well as the ground state and arrange the eigenstates in the same order as the standard map.

Figure 14(b) gives the splitting ΔE_0 as a function of $1/h$. For $\varepsilon > 0$, the splitting decays exponentially accompanied with periodic spikes. All the features have clearly been accounted for if one applies the semiclassical method using complex paths [19]. The spikes appear as a result of the energetic resonance between the states localized in the inner well and outer region. The coupling strength could be evaluated using the imaginary action of complex trajectories which bridge classical disjointed equi-energy surfaces.

It would be worth mentioning that for $\varepsilon = 0$ the condition $H(q, p) = 0$ can be factorized into

$$\cos^2 q + \cos^2 p = 0, \quad (21)$$

and

$$\cos^2 q + \cos^2 p = -1/2a. \quad (22)$$

This shows that the invariant curves specified by (21) and (22) are not connected even in the complex plane, thus no tunneling connection between the inner and outer

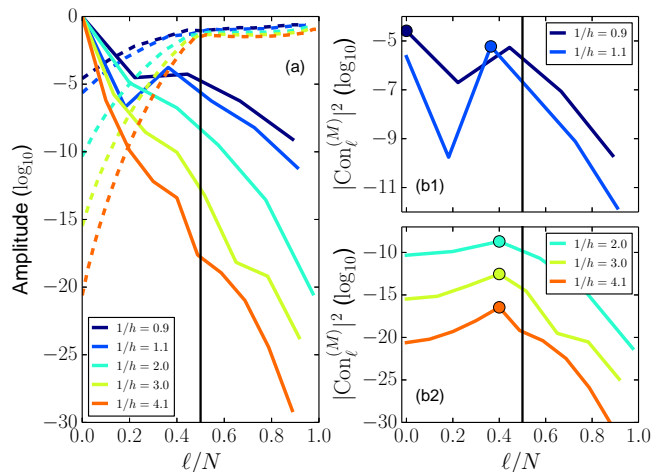


FIG. 15: (Color online) (a) The amplitude of $\langle q|\Psi_\ell\rangle$ at $q = 0$ (dashed curves) and the action representation $\langle J_n|\Psi_0\rangle$ (solid curves) as a function of the normalized quantum number ℓ/N . Right panels give the contribution spectrum $\text{Con}_\ell^{(M)}$ (\log_{10}) as a function of the normalized quantum number ℓ/N for (b1) a small $1/h$ regime, and (b2) a semiclassical regime.

regions exists even though both are the surfaces with the same energy [33]. As a result, the splitting ΔE_0 exhibits single exponential decay without spikes.

On the other hand, with careful observation of the splitting curve for $\varepsilon > 0$ (see Fig. 14(b)), we notice that there exists a crossover from one slope to another. In a small $1/h$ regime, the slope can be well fitted by the one for $\varepsilon = 0$, whereas the best fit curve, colored in gray in Fig. 14(b), shows another slope in the large $1/h$ regime.

Such a crossover or the change of the slope of the splitting curve reminds us of the plateau discussed in the nonintegrable situation. However, the origin and the underlying mechanism entirely differs from the previous one. This can be confirmed again by examining the contribution spectrum. Here we use the eigenstates $|J_n\rangle$ as the basis states for the contribution spectrum, where $\hat{H}_0(\hat{q}, \hat{p})|J_n\rangle = E_n^{(0)}|J_n\rangle$.

As shown in Fig. 15(b1), a switching from the instanton to another mode also occurs, like the standard map case. However, in the integrable case, the position of the peak sits at the same value of ℓ/N and does not move even if the value of $1/h$ is changed, while remember that it depends on $1/h$ and shift leftwards in case of the standard map. Note here that ℓ/N can be identified with the action coordinate. The reason for the peak position being fixed is simple; the peak appears as a result of the coupling between inner and outer surface, which is expected to occur in the RAT scenario. Alternatively stated, the origin of coupling is purely classical. Furthermore, as shown in Fig. 16, the leading-order semiclassical ansatz, which was discussed in the previous section, works quite well for the eigenfunction in the action representation. These results make a sharp contrast to the standard map

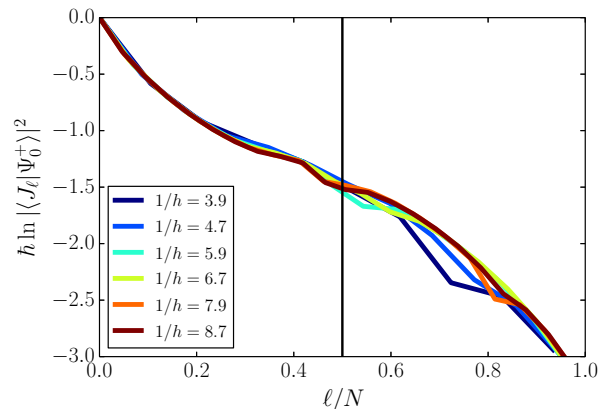


FIG. 16: (Color online) Scaled wavefunction $\hbar \ln |\langle J_\ell|\Psi_0^+\rangle|^2$ as a function ℓ/N for several effective Planck's constant h , each of which is taken at the values of off resonance positions in Fig.15(b).

case. We can see in Fig. 17 that the maximal mode in the contribution spectrum well reproduces the structure of eigenfunction around $q = 0$, and its support is exactly an invariant curve with the same energy as that of the ground state.

The presence of the crossover admits a simple semiclassical interpretation. As discussed in [19], there exist two different complex paths with different imaginary actions. One corresponds to the ordinary instanton path, which runs from one well to another directly and the other is the path bypassing the classical resonance chain. In the semiclassical regime, since the latter one has a smaller imaginary action. On the other hand, in a small ε regime, it can happen that the instanton contribution is larger than that from the bypassing one, in spite of the magnitude relation of imaginary actions. This is because the prefactor, more precisely the coupling amplitude due to tunneling, comes into play in a relatively small $1/h$ regime. The observed crossover would be understood by taking into account not only the imaginary action but the coupling amplitude. This argument suggests that, in a larger ε regime, the coupling with bypassing path gets larger, and the crossover point disappears when the value of ε exceeds a certain threshold. Note, however that the splitting curve cannot form the staircase structure since we have at most two possible complex paths, and the underlying mechanism generating spikes has a purely classical origin as stated above.

VI. SUMMARY AND OUTLOOK

The focus of the present paper was put on clarifying the origin of the enhancement of tunneling probability in the nearly integrable system. We here measured the tunneling probability by observing tunneling splittings plotted as a function of the inverse Planck's constant. Typical

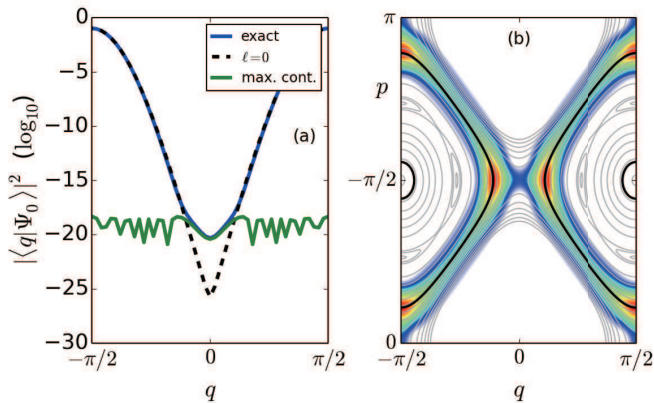


FIG. 17: (Color online) (a) The eigenfunction $|\Psi_0\rangle$ in the q -representation for $\varepsilon = 5/1000$ (blue), the eigenfunction $|J_0\rangle$ (dotted) and the maximal mode in the contribution spectrum at $q = 0$ (green), respectively. (b) The maximal mode state in the Husimi representation for $h = 1/5$. The black thick curves represent inner and outer invariant curves with the same energy $E = E_0$.

features of the splitting curve commonly observed in non-integrable quantum maps are the existence of spikes and persistent departure of the splitting curve from the one predicted by the instanton.

So far these have been discussed in the framework of RAT theory, but here we took a different perspective: the splitting curve is composed of the staircase-shaped backbone accompanied by spikes. We have observed that, by introducing the absorber composed of integrable bases, spikes could be selectively suppressed if states interacting with the reference doublet are absorbed. More precisely, we have shown that the interacting or third state could be decoupled from the reference doublet when we take an integrable state that has maximally overlap with the corresponding eigenstate as the absorber. The eigenenergy of such eigenstates responsible for generating spikes are pushed out to the complex plane, and spikes disappear. Our observation was that even though all the third states which resonate energetically with the reference doublet are suppressed in such a way the staircase structure survives. Note that the efficiency of the present absorber comes from the fact that the regime we consider is close enough to the integrable limit, otherwise the absorber may affect irrelevant states in an uncontrollable way.

The result strongly suggests the existence of non-trivial broad interaction between the reference doublet and other states. This was indeed confirmed by introducing renormalized Hamiltonian, which is constructed using the BCH expansion, and used as basis states by which the reference state is expanded. In particular, we focus on the contribution spectrum at the origin $q = 0$ since the amplitude of eigenfunctions at the origin follows the behavior of tunneling splitting. Here the contribution spectrum introduced in [21] represents components of renormalized states in the reference state.

The contribution spectrum analysis clearly revealed that, in addition to the self component representing the instanton, there certainly exists broad interaction, and the behavior of such broadly spread components controls the staircase structure in the splitting curve. There are two key ingredients to explain the emergence of the staircase: one is the behavior of the most dominant state in broad components, the other is anomalous tail observed in the eigenfunction in the action representation. Note that the renormalized bases are crucially important to capture these features, otherwise one could not explain the existence of the staircase structure and the anomalous tail part in the action representation as well.

The dominant contributor in the broadly spread components switches from one to another, which was observed in the contribution spectrum. Such a switching phenomenon is driven by and linked to the existence of the fundamental energy sequence, which is further enhanced when the quantum resonance between unperturbed system and the periodic driving occurs.

The origin of anomalous part in the action representation should be explored more closely, which will become a primary subject of our forthcoming papers. The semiclassical analysis based on the correspondence principle, in which not complex but real classical orbits are used as input information. This efficiently works and turns out to extract anomalous components in classical dynamics of the BCH Hamiltonian [30]. The analogy with the system modeling the diffraction, together with some speculations on anomalous behaviors of caustics appearing in the semiclassical analysis will be another approach [32]. The latter suggests that observed phenomena in the eigenfunction in the action representation are beyond the leading semiclassical description.

These two key characteristics are, by their very nature, absent in the completely integrable system. Therefore, one could predict that the staircase structure does not appear in the completely integrable. We have confirmed this for a normal form Hamiltonian system, for which the validity of RAT theory was recently investigated. We have shown that a sharp contrast exists between integrable and nonintegrable systems and verified that the dominant contributor in the contribution spectrum for the integrable system sits at the same position and does not move as in the nonintegrable case. The absence of the staircase structure could simply be interpreted by the fact that there exists a unique dominant complex path in the semiclassical regime.

Finally we would like to emphasize the importance of observing wavefunctions in the whole range, not focusing only on the amplitude at a specific point, like the origin $q = 0$ in the present case. As discussed in subsection IV A, with increase in $1/h$, the convex structure around the origin, appearing in the first plateau, is pushed outward and forms shoulders in both sides. The same process happens repeatedly as one further increases $1/h$, that is, similar shoulders appear one after another. In this sense, we can find the trace of the staircase of the split-

ting curve in the tail pattern of wavefunction. This is also true for wavefunction in the action representation. There exists a significant difference between inner and outer tunneling tail, and this exactly results in different slopes of the splitting curve and thus staircase skeleton.

ACKNOWLEDGMENTS

We are grateful for useful discussions with H. Harada, J. Le Deunff, A. Mouchet, T. Okushima, and K. Taka-

hashi. We especially thanks to N. Mertig for his helpful comments on RAT theory. This work has been supported by JSPS KAKENHI Grant Numbers 24340094 and 25400405. The authors appreciate Shoji Tsuji and Kankikai for using their facilities at Kawaraya during this study.

-
- [1] S. C. Creagh, *Tunneling in two dimensions* in *Tunneling in Complex Systems*, edited by S. Tomsovic (World Scientific, 1998), p. 35.
- [2] S. Keshavamurthy and P. Schlagheck, *Dynamical Tunneling: Theory and Experiment*, (CRC Press 2011).
- [3] W. A. Lin and L. E. Ballentine, Phys. Rev. Lett. **65**, 2927 (1990).
- [4] O. Bohigas, S. Tomsovic and D. Ullmo, Phys. Rev. Lett. **65**, 5 (1990).
- [5] S. Tomsovic and D. Ullmo, Phys. Rev. E **50**, 145 (1994).
- [6] R. Roncaglia, L. Bonci, F. M. Izrailev, B. J. West and P. Grigolini, Phys. Rev. Lett. **73**, 802 (1994).
- [7] L. Bonci, A. Farusi, P. Grigolini and R. Roncaglia, Phys. Rev. E **58**, 5689 (1998).
- [8] O. Brodier, P. Schlagheck and D. Ullmo Phys. Rev. Lett. **87**, 064101 (2001); Ann. Phys. **300**, 88 (2002).
- [9] C. Eltschka and P. Schlagheck, Phys. Rev. Lett. **94**, 014101 (2005).
- [10] A. Mouchet, C. Eltschka, and P. Schlagheck, Phys. Rev. E **74**, 026211 (2006).
- [11] S. Löck, A. Bäcker, R. Ketzmerick and P. Schlagheck, Phys. Rev. Lett. **104**, 114101 (2010).
- [12] P. Schlagheck, A. Mouchet and D. Ullmo, in *Dynamical Tunneling: Theory and Experimental*, edited by S. Keshavamurthy and P. Schlagheck (CRC Press, 2011) Vol. 8, p. 177. (CRC Press, 2011)
- [13] S. Coleman, *The uses of instanton* in *Aspects of Symmetry: Selected Erice Lectures* (Cambridge University Press, 1988), Vol. 7, p. 265.
- [14] A. Shudo and K. S. Ikeda, Prog. Theor. Phys. Supple. **116**, 283 (1994); Physica D **115** 234 (1998).
- [15] A. Shudo, Y. Ishii and K. S. Ikeda, J. Phys. A **42**, 265101 (2009); 265102 (2009)
- [16] M. Wilkinson, Physica D **21**, 341 (1986).
- [17] S. C. Creagh, J. Phys. A **27**, 4969 (1994).
- [18] J. Le Deunff and A. Mouchet, Phys. Rev. E **81**, 046205 (2010).
- [19] J. Le Deunff, A. Mouchet and P. Schlagheck, Phys. Rev. E **88**, 042927 (2013).
- [20] A. Shudo and K. S. Ikeda, Phys. Rev. Lett. **109**, 154102 (2012).
- [21] A. Shudo, Y. Hanada, T. Okushima and K. S. Ikeda, Europhys. Lett. to be published.
- [22] B. V. Chirikov, Phys. Rep. **52**, 263 (1979).
- [23] In the vicinity of the energy corresponding to the unstable fixed point at $(q, p) = (0, 0)$, the states $|\Psi_n^\pm\rangle$ do not form tunneling doublets, so this numbering rule does not work, but this ambiguity will not cause any serious confusion in the present description.
- [24] L. Kaplan, Phys. Rev. E **59**, 5325 (1999).
- [25] D. Lippolis, J.-W. Ryu, S.-Y. Lee and S. W. Kim, Phys. Rev. E **86**, 066213 (2012).
- [26] J. P. Keating, S. Nonnenmacher, M. Novaes and M. Sieber, Nonlinearity **21**, 2591 (2008).
- [27] A. Bäcker, R. Ketzmerick and S. Löck, Phys. Rev. E **82**, 056208 (2010).
- [28] N. Mertig, Ph.D. thesis, Technische Universität Dresden, 2013.
- [29] R. Scharf, J. Phys. A **21** 2007 (1988).
- [30] A. Shudo, Y. Hanada, T. Okushima and K. S. Ikeda in preparation.
- [31] A. Ishikawa, A. Tanaka, K. S. Ikeda and A. Shudo, Phys. Rev. E **86**, 036208 (2012).
- [32] Y. Hanada, A. Shudo and K. S. Ikeda in preparation.
- [33] H. Harada and A. Shudo, private communications.
- [34] In Eq. (5) we drop suffices \pm since the definition of \hat{P} makes sense irrespective of the symmetry.